2014

Single-phase Flow Pressure Drop of R134a Vapor and Liquid in the Vertical Header of Multi-Pass Microchannel Heat Exchanger

Yang Zou
University of Illinois at Urbana-Champaign, United States of America, yangzou1@illinois.edu

Predrag S. Hrnjak
pega@illinois.edu

Single-phase Flow Pressure Drop of R134a Vapor and Liquid in the Vertical Header of Multi-Pass Microchannel Heat Exchanger

Yang ZOU[1,2], Pega HRNJAK[1,2]*

[1]University of Illinois at Urbana-Champaign, Department of Mechanical Science and Engineering, Urbana, IL, USA

[2]Creative Thermal Solutions
Urbana, IL, USA
Contact Information (1-217-244-6377, yangzou1@illinois.edu, pega@illinois.edu)

* Corresponding Author

ABSTRACT

Refrigerant maldistribution in the microchannel heat exchanger (MCHX), though mainly due to phase separation in the header in two-phase flow, is also affected by the pressure drop in the header. This paper investigates the single-phase flow pressure drop of nitrogen, R134a vapor, and R134a liquid in the vertical header of a multi-pass microchannel heat exchanger. The objective is to develop a model for the single-phase pressure drop in the header and provide the basis for two-phase flow pressure drop model. The fluid enters into the vertical header through five microchannel tubes in the bottom pass and exits through five microchannel tubes in the top pass representing the flow in the outdoor MCHX of a reversible system under heat pump mode. The local pressure drop across each exit microchannel tube in the header is measured at various inlet mass flow rates. For nitrogen and R134a vapor, the local pressure drop usually reduces along the upward flow in the header. For R134a liquid, the local pressure drop is highest across the second exit tube, and then it decreases along the upward flow. The measured overall local pressure drop includes the acceleration, gravitation, friction, and minor pressure drop due to the protruded microchannel tube. The minor pressure drop coefficient based on the experimental results is compared with the empirical correlation. It is found that the empirical correlation works well for nitrogen and R134a vapor but not for R134a liquid. A new correlation for R134a liquid is proposed with the same format, but the coefficients are derived based on the experimental results of this study using the least square curve-fit method.

1. INTRODUCTION

The outdoor multi-pass microchannel heat exchanger (MCHX) of a reversible system, usually having vertical headers and horizontal tubes, is widely used in automotive and residential air-conditioning systems, for the advantages in higher heat transfer, compactness, and possible charge reduction. In heat pump (HP) mode, the outdoor MCHX functions as an evaporator and refrigerant maldistribution creates unwanted superheated region where the heat transfer is lower than the two-phase flow region due to the lower heat transfer coefficient of the superheated vapor and less temperature difference between refrigerant and air. Thus, refrigerant maldistribution deteriorates the MCHX performance, and consequently reduces the system efficiency. Byun and Kim (2011) presented R410A maldistribution in a two-pass outdoor MCHX under HP mode caused the cooling capacity reduced up to 13.4% compared to the uniform distribution case. Zou et al. (2014) showed capacity degradation of up to 30% and 5% for R410A and R134a maldistribution in a two-pass outdoor MCHX under HP mode, respectively.

The knowledge to achieve good distribution is still limited, though it has been extensively studied. Fei and Hrnjak (2002), Vist and Pettersen (2004), Webb and Chung (2005), Bowers et al. (2006), and Hwang et al. (2007) examined refrigerant distribution in the horizontal headers with vertical parallel tubes, which usually appeared in the indoor microchannel heat exchangers. Watanabe et al. (1995), Cho and Cho (2004), Lee (2009), Byun and Kim (2011), and

Zou and Hrnjak (2013a, 2013b, 2014) investigated the two-phase flow in the inlet and/or intermediate vertical header, which were commonly used in the outdoor heat exchangers and the distribution became important when it was used as an evaporator in HP mode. These studies showed that the phase separation between liquid and vapor in the header, which was affected by several conditions (e.g. header geometry and orientation, fluid properties, and inlet conditions), had a strong influence on the flow regime in the header and refrigerant distribution among the parallel branch tubes in two-phase flow.

However, refrigerant distribution is also affected by the distribution of pressure drop in the heat exchanger. Because of several parallel microchannel tubes, there are numerous flow paths in the heat exchanger. Each flow path starts from the inlet of the heat exchanger and ends at the outlet of the heat exchanger; thus, the pressure drop along each flow path is equal. For example, if along one path the pressure drop in the header is greater than along another flow path, the pressure drop in the tube must be lower, resulting in the lower mass flow rate in that tube. This situation affects refrigerant distribution in addition to quality distribution in the header at the entrance of each tube, which is mainly a result of two-phase flow regime in the header.

In the first pass of a multi-pass MCHX, it may be single-phase subcooled liquid supplied into the inlet header (by flash gas bypass in Tuo and Hrnjak (2014)); while in the last pass, it may be single-phase superheated vapor in the header. Although there is no phase separation in these two cases because of the single-phase flow, refrigerant maldistribution among parallel microchannel tubes still exists due to the pressure drop in the header, as reported by Yin et al. (2002). Tuo and Hrnjak (2014) presented that such single-phase maldistribution in a MCHX with horizontal headers also significantly affected the heat exchanger and system performance. Yin et al. (2002) developed a single-phase pressure drop model for the whole microchannel heat exchanger based on the experimental results of nitrogen. Ren and Hrnjak (2014) examined the pressure drop of single-phase compressed air in the horizontal header and improved the pressure drop model of Yin et al. (2002) based on their experimental results.

2. EXPERIMENTAL METHOD

The test rig was constructed to study R134a distribution in a MCHX with vertical headers, as shown in Figure 1. The single-phase R134a liquid was pumped into the inlet header. Going through the five microchannel tubes in the bottom pass, liquid entered into the test header. Due to maldistribution, different amount of liquid exited through the microchannel tubes in the top pass, where the mass flow rate in each tube was individually measured. For supplying nitrogen or single-phase R134a vapor to the test section, the section from condenser to gear pump was bypassed. The nitrogen or single-phase R134a vapor was supplied from a pressurized cylinder at a point after the gear pump and exited the system to the atmosphere at a point before condenser. The local pressure drop across each exit microchannel tube, as shown in Figure 1, was measured by Rosemount differential pressure transmitter (0 to 3 in WC, 0.25% FS). The mass flow rate in each outlet microchannel tube was measured by Micro Motion DS06 flow meter (±0.15%).

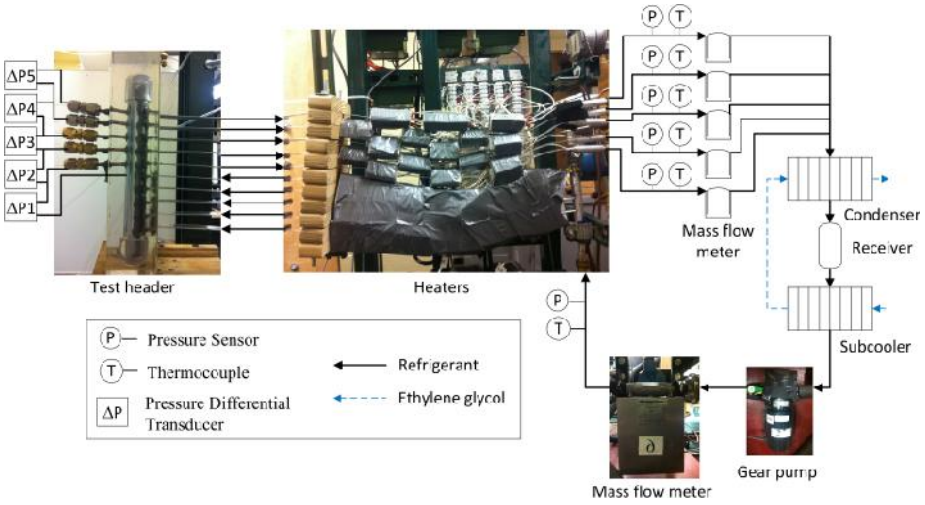

Figure 1: System schematics

The uncertainty propagation analysis (e.g. for pressure loss coefficient) was carried out in the EES (2012). It was based on Equation (1). The uncertainty is presented with the error bars in the figures of next section.

$$¢U = \sqrt{\sum_{i=1}^{N}\left(\frac{\partial U}{\partial y_i}\right)^2 ¢y_i^{\,2}} \quad \text{where } U = U(y_1, y_2, y_3, ...) \tag{1}$$

The transparent circular header, made of the PVC tube, had five inlet and five exit microchannel tubes protruded into the ½ depth of header's inner diameter. The geometries of the transparent header and aluminum microchannel tube are listed in Table 1. The test conditions are shown in Table 2.

Table 1: Vertical header and microchannel tube geometries

Item	Data
Header geometry	
Inner diameter	15.44 mm
Header length	170 mm for 5+5 header; 300mm for 10+10 header
Tube pitch	13 mm
Tube protrusion	½ depth and ¾ depth of inner diameter
Microchannel geometry	
Shape	Rectangular
Number of ports	17
Length	0.54 mm
Width	0.5 mm
Hydraulic diameter	0.5 mm

Table 2: Test conditions

Item	Data
Saturation temperature	25 ºC for nitrogen and R134a vapor; 5 ºC for R134a liquid
Inlet mass flow rate	2.14 – 4.19 g s^{-1} for nitrogen and R134a vapor 2.14 – 6.25 g s^{-1} for R134a liquid

3. RESULTS AND DISCUSSION

3.1 Nitrogen and R134a vapor pressure drop

The distribution of R134a vapor (compared with nitrogen) at various inlet mass flow rate is shown in Figure 2. It is noticed that the distribution is not uniform even though the fluid is single-phase. The bottom tube has the highest flow rate. It reduces as the flow goes up, due to the pressure drop in the header. Tube #1 is closest to the inlet (in this case, in the middle of the header). The outlet state is the same for each tube, and thus Tube #1 has the highest pressure difference in the tube because the fluid experiences the shortest distance in the header (i.e. lowest pressure drop in the header). Therefore, the mass flow rate in Tube #1 is highest corresponding to the highest pressure difference in the tube. For the other tubes, as the fluid experiences longer distance in the header, the pressure difference in the tube becomes lower so that the mass flow rate in the tube is lower. For the last top tube, it is farthest from the inlet. It experiences the highest pressure drop in the header, i.e. the sum of ΔP_1, ΔP_2 to ΔP_5. Thus, the pressure difference and mass flow rate in Tube #5 is the lowest.

Figure 3 presents the local pressure drop in the header across each exit microchannel tube. The pressure drop of R134a vapor is lower than that of nitrogen because the density of R134a vapor is much higher than that of nitrogen; thus, the velocity of R134a vapor is lower while the mass flow rate in each section of the header is similar. As R134a vapor or nitrogen branches out, the mass flow rate in the header is reduced. Therefore, the velocity and local pressure drop also reduces along the upward flow. The pressure drop in Location #5 may be higher than that in Location #4. This may be due to that there is no flow at the end of the header and it is stagnation pressure at the top.

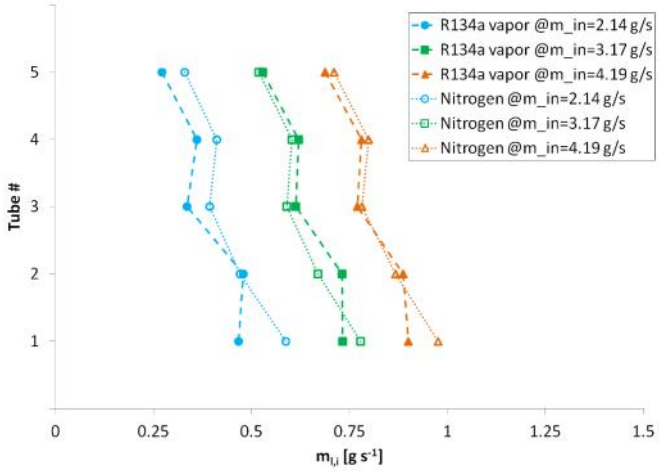

Figure 2: Maldistributions of nitrogen and R134a vapor

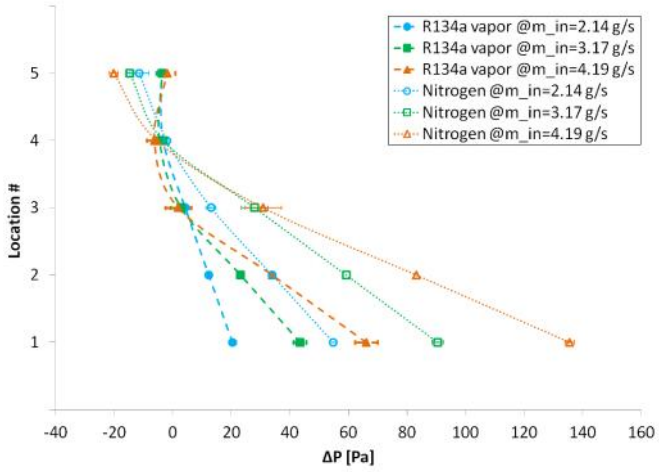

Figure 3: Local pressure drop in the header (nitrogen and R134a vapor)

The overall pressure drop in the header includes acceleration, gravitation, friction and minor pressure drop due to tube protrusion, as in Equation (2). Ren and Hrnjak (2014) investigated the pressure drop of compressed air in a horizontal header and proposed Equation (3) - (6) to calculate the acceleration, gravitation, friction, and minor pressure drop, respectively. The density in Equation (3) to Equation (6) is constant and estimated based on the pressure in the header. For friction pressure drop, the equations for Darcy friction factor are from White (2008). The notations for S_{eff} and S_{tot} are shown in Figure 4. The hydraulic diameter D_h is calculated at the smallest cross section area, i.e. enclosed by S_{eff} and S_t. For the minor pressure drop coefficient, based on their results of compressed air in the horizontal header, Ren and Hrnjak (2014) proposed a set of empirical equations, as shown in Equation (7).

$$\Delta P = \Delta P_{acc} + \Delta P_{gra} + \Delta P_{fri} + \Delta P_{pro} \tag{2}$$

$$\Delta P_{acc} = °v_2^2 - °v_1^2 \tag{3}$$

$$\Delta P_{gra} = °gl \tag{4}$$

$$\Delta P_{fri} = f_1 \frac{l/2}{D_h} \frac{S_{eff}}{S_{tot}} \circ v_1^2 + f_2 \frac{l/2}{D_h} \frac{S_{eff}}{S_{tot}} \circ v_2^2 \tag{5}$$

where $$f = \begin{cases} \dfrac{0.3164}{\mathrm{Re}^{1/4}} & 4000 < \mathrm{Re} < 10^5 \\ (1.8 \log \dfrac{\mathrm{Re}}{6.9})^{-2} & \mathrm{Re} > 10^5 \end{cases}$$

$$S_{tot} = S_{eff} + S_t$$

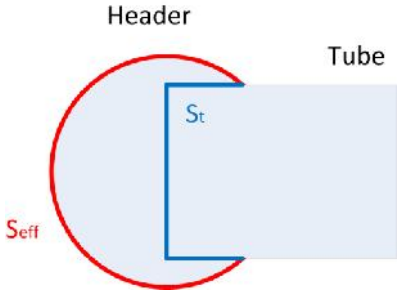

Figure 4: Parameter notation for Equation (5)

$$\mathrm{a}P_{pro} = \text{¸} \circ \frac{v_1^2}{2} \tag{6}$$

$$\zeta = \begin{cases} 0.75\, exp\left(-14.582 \dfrac{v_{t,i}}{v_{M,i}} + 4.017 \right) + 0.111 \left(\dfrac{v_{t,i}}{v_{M,i}} \right)^2 \\ \quad - 0.218 \dfrac{v_{t,i}}{v_{M,i}} & if\ i = 1 \\ -0.4\, exp\left(-24.230 \dfrac{v_{t,i-1}}{v_{M,i-1}} + 7.261 \right) + 0.242 \dfrac{v_{t,i}}{v_{M,i}} & \\ \quad - 0.031 v_{t,i} + 0.269 & if\ i = 2 \\ 0.297 \dfrac{v_{t,i}}{v_{M,i}} - 0.044 v_{t,i} + 17.340\, exp(-1.715 \bullet i) & \\ \quad + 0.165 & if\ i \geq 3 \end{cases} \tag{7}$$

In this study, Equations (3) - (5) are used to calculate the acceleration, gravitation, and friction pressure drops. The minor pressure drop due to protruded tube is obtained by subtracting the calculated acceleration, gravitation and friction pressure drop from the measured overall pressure drop. Figure 5 presents each component of the pressure drop. The acceleration and minor pressure drops are main components of the overall pressure drop. The minor pressure loss coefficient is calculated based on the experimental results using Equation (6), then compared with Equation (7) in Figure 6. It is found that only at Location #1, the values are very close. In other locations, it usually deviates by 30% to 200%. As the flow moves downstream, the difference becomes larger.

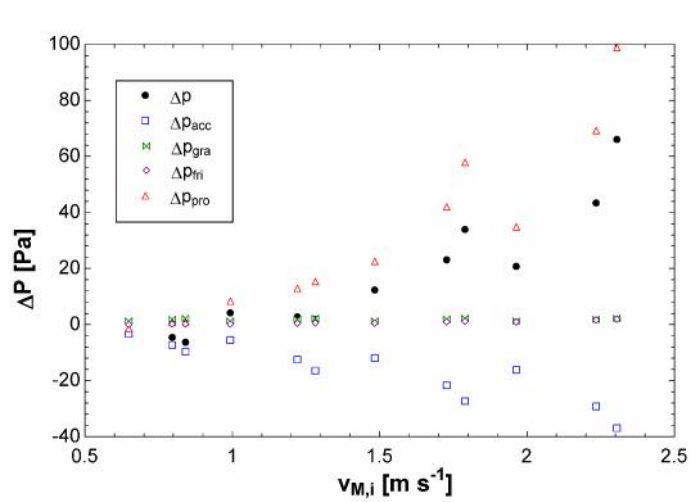

Figure 5: Overall, acceleration, gravitation, friction, and minor pressure drops (R134a vapor)

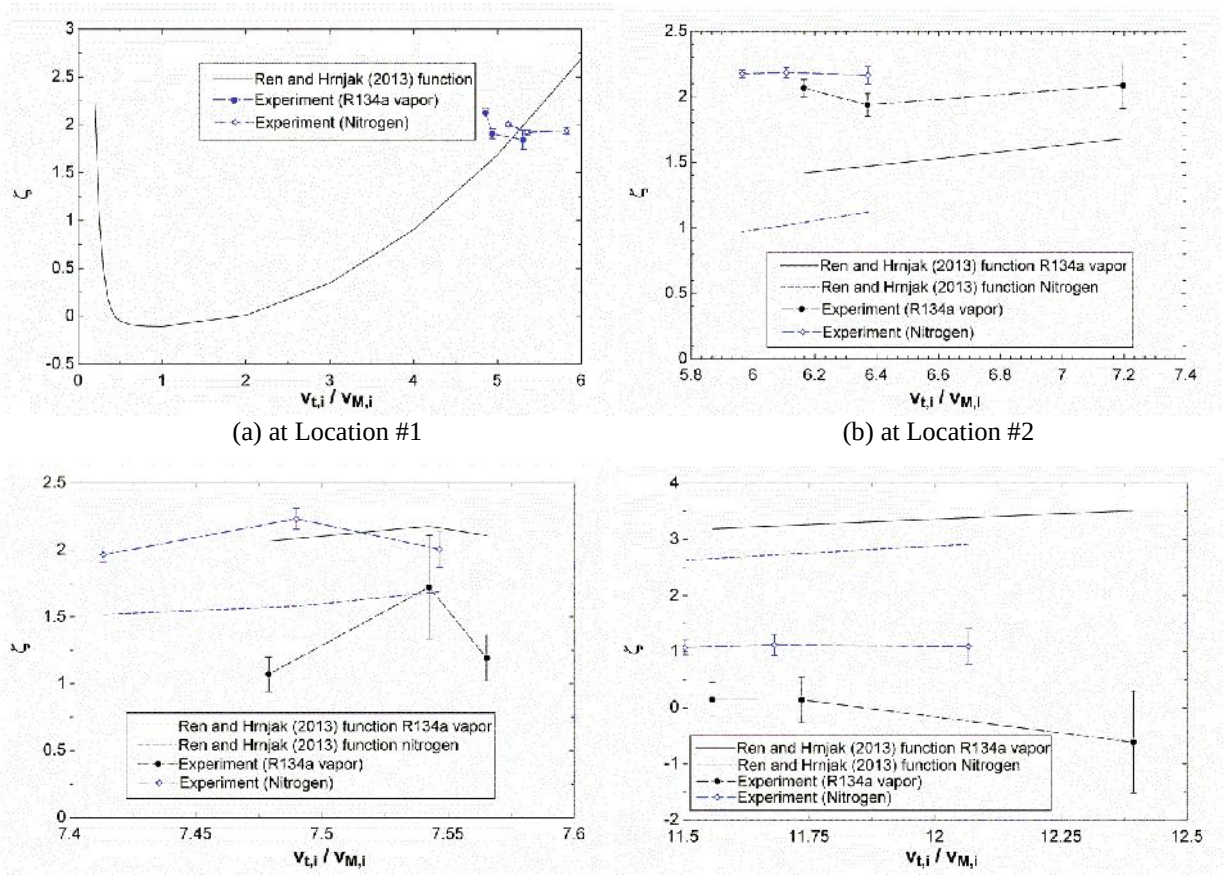

(a) at Location #1 (b) at Location #2

(c) at Location #3 (d) at Location #4

Figure 6: Minor pressure loss coefficient (nitrogen and R134a vapor)

However, in the header, the most significant minor pressure drop is in the first few tubes, as shown in Figure 3, because the flow rate over there is higher. Although the minor pressure loss coefficient correlation in Equation (7) deviates from the measured values in the last few tubes, it does not affect too much on the minor pressure drop calculation. The predicted minor pressure drop is compared with the experimental results in Figure 7. By comparing Figure 7(a) with Figure 7(b), it can be conceived that Equation (7) predicts better than using $\zeta = 0.2$ as reported in Yin et al. (2002). The deviation of Equation (7) from the experiment result is usually within ±15 Pa, especially for R134a vapor, which is within the accuracy range reported by Ren and Hrnjak (2014).

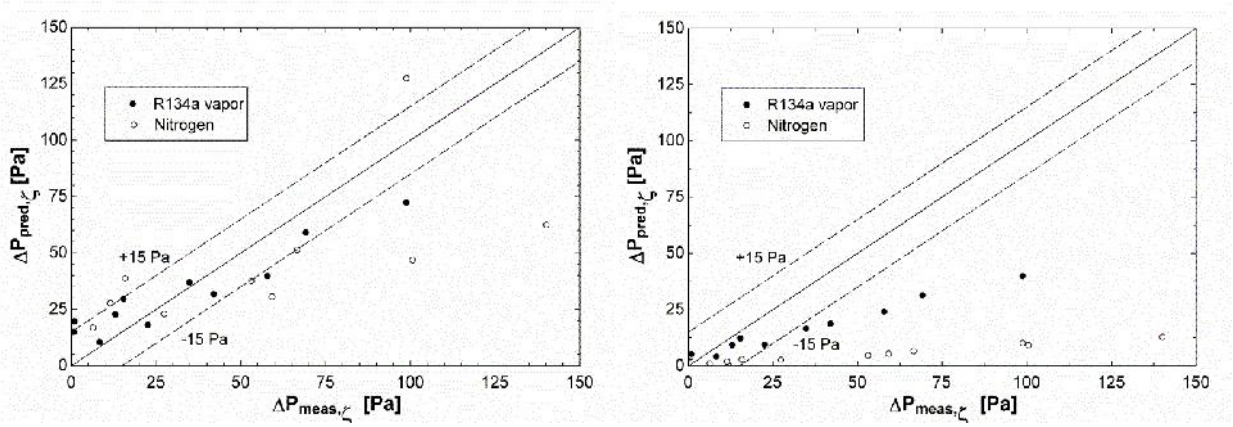

(a) Equation (7) from Ren and Hrnjak (2014) (b) ζ = 0.2 from Yin et al. (2002)

Figure 7: The predicted minor pressure drop vs. the measured minor pressure drop (nitrogen and R134a vapor)

3.2 R134a liquid pressure drop

Similarly, for single-phase R134a liquid, the pressure drop in the header causes the flow rate maldistribution among the microchannel tubes, as shown in Figure 8. The bottom tubes have higher mass flow rate than the top tubes. The local pressure drop in the header is presented in Figure 9. In Figure 9, the pressure drop across the second or third exit tube is highest in the header. As the flow goes downstream, the pressure drop decreases.

The same method using Equation (2) – (6) are applied to analyze each component of the measured overall pressure drop of single-phase liquid. Unlike the case of R134a vapor, for R134a liquid, the most important components of the overall pressure drop are gravitation and minor pressure drops, as shown in Figure 10. As shown in Figure 10(a), the prediction of the minor pressure drop based on Equation (7) does not work well for single-phase liquid. It deviates significantly from the measured minor pressure drop. The new set of equations for calculating the minor pressure loss coefficient of single-phase liquid are derived, as shown in Equation (8). The same format as Equation (7) is used, but the coefficients in Equation (8) are obtained by curve-fitting the experimental results of R134a liquid based on least square method. Figure 10(b) shows that the prediction of Equation (8) is better; most data are within ±15 Pa of the measured minor pressure drop.

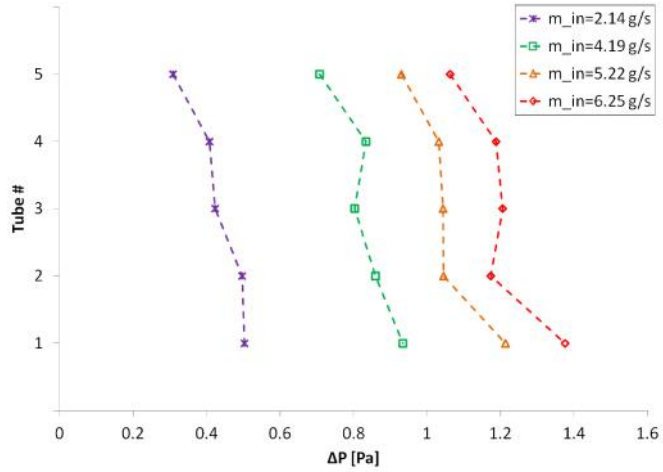

Figure 8: Maldistribution of R134a liquid

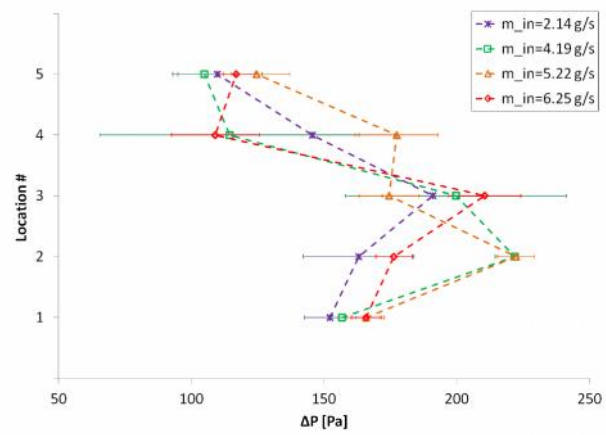

Figure 9: Local pressure drop in the header (R134a liquid)

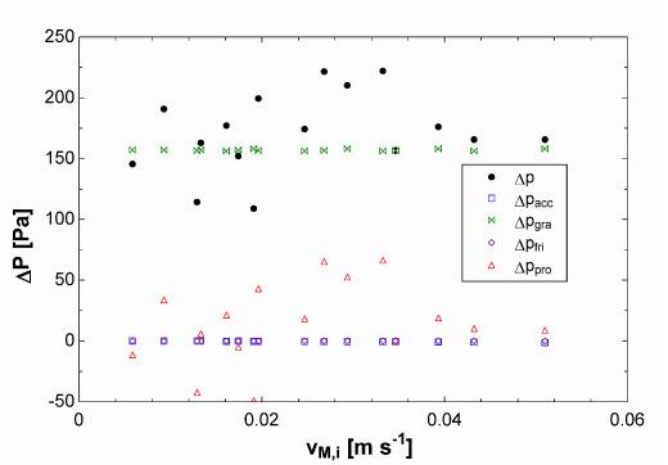

Figure 9: Overall, acceleration, gravitation, friction and, minor pressure drops (R134a liquid)

$$, = \begin{cases} 0.616\exp\left(0.959\dfrac{v_{t,i}}{v_{M,i}}+0.551\right)-3.724\left(\dfrac{v_{t,i}}{v_{M,i}}\right)^2 \\ -5.690\dfrac{v_{t,i}}{v_{M,i}} \qquad if\ i=1 \\ -31.875\exp\left(-92.370\dfrac{v_{t,i-1}}{v_{M,i-1}}+453.187\right) \\ +113.216\dfrac{v_{t,i}}{v_{M,i}}-802.277v_t-412.364 \quad if\ i=2 \\ -666.473\dfrac{v_{t,i}}{v_{M,i}}-137.879v_t+1.351\exp(2.749\bullet i) \\ +0.562 \qquad if\ i\geq 3 \end{cases} \tag{8}$$

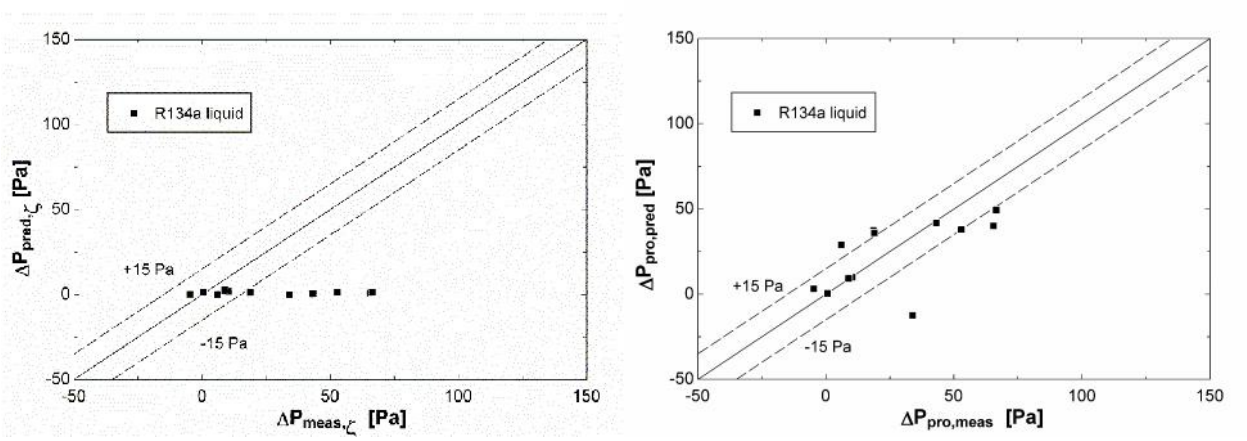

(a) Equation (7) from Ren and Hrnjak (2014) (b) Equation (8)

Figure 10: The predicted minor pressure drop vs. the measured minor pressure drop (R134a liquid)

4. CONCLUSIONS

This paper investigated the pressure drop in the vertical header of R134a vapor (compared with nitrogen) and R134a liquid. Maldistribution exists even in single-phase fluid flow. This is caused by the pressure drop in the header, which includes acceleration, gravitation, friction, and minor pressure drop due to tube protrusion. The previously reported correlation in Ren and Hrnjak (2014) works well to calculate the minor pressure drop of R134a vapor (and nitrogen). However, for R134a liquid, Ren and Hrnjak (2014) correlation does not work very well, and a new set of empirical equations is derived based on the experimental results in this study.

NOMENCLATURE

D_h	Hydraulic diameter (m)	Subscripts	
f	Darcy friction factore	acc	Acceleration ΔP
g	Gravity acceleration (m s^{-2})	fri	Friction ΔP
l	Tube pitch (m)	gra	Gravitation ΔP
m	Mass flow rate (g s^{-1})	i	Branch number
P	Pressure (kPa)	in	At the smallest area in the middle of the header
Re	Reynolds number		
T	Temperature (K)		
S_{eff}	Effective perimeter	l	liquid
S_t	Tube (in the header part) perimeter	pro	Minor ΔP
S_{tot}	Total perimeter including protruded tube	v	vapor
v	Velocity (m s^{-1})		
δU	Uncertainty		
y	Parameter		
ΔP	Pressure drop (Pa)		
ρ	Density (kg m^{-3})		
ζ	Minor pressure loss coefficient		

REFERENCES

Bowers, C.D., Hrnjak, P.S., Newell, T.A., 2006. Two-phase refrigerant distribution in a micro-channel manifold. *Proc. 11th Int. Refrigeration Air Conditioning Conf. at Purdue*, R161.

Byun, H.W., Kim, N.H., 2011. Refrigerant distribution in a parallel flow heat exchanger having vertical headers and heated horizontal tubes. *Exp. Thermal Fluid Sci.* 35, 920-930.

Cho, H., Cho, K., 2004. Mass flow rate distribution and phase separation of R-22 in multi-microchannel tubes under adiabatic condition. *Microscale Thermophysical Eng.* 8 (2), 129-139.

Fei, P., Hrnjak, P.S., 2004. Adiabatic Developing Two-Phase Refrigerant Flow in Manifolds of Heat Exchangers. *Technical Report TR-225, Air Conditioning and Refrigeration Center, Univ. Illinois at Urbana-Champaign.*

Hwang, Y., Jin, D.H., Radermacher, R., 2007. Refrigerant distribution in minichannel evaporator manifolds. *HVAC&R Res.* 13 (4), 543-555.

Lee, J.K., 2009. Two-phase flow behavior inside a header connected to multiple parallel channels. *Exp. Thermal Fluid Sci.* 33, 195-202.

Ren, T., Hrnjak, P.S., 2014. Pressure drop in round cylindrical headers of parallel flow MCHXs: pressure loss coefficient for single phase flow. *Int. J. Refrigeration.* In Press.

Tuo, H., Hrnjak, P.S., 2014. Effect of the header pressure drop induced flow maldistribution on the microchannel evaporator performance. *Int. J. Refrigeration.* 36, 2176-2186.

Vist, S., Pettersen, J., 2004. Two-phase flow distribution in compact heat exchanger manifolds. *Exp. Thermal Fluid Sci.* 28, 209-215.

Watanabe, M., Katsuta, M., Nagata, K., 1995. General characteristics of two-phase flow distribution in a multipass tube. *Heat Transfer-Japanese Res.* 24, 32-44.

Webb, R.L., Chung, K., 2005. Two-phase flow distribution to tubes of parallel flow air-cooled heat exchangers. *Heat Transfer Eng.* 26 (4), 3-18.

Yin, J.M, Bullard, C.W., Hrnjak, P.S., 2002. Single-phase pressure drop measurements in a microchannel heat exchanger. *Heat Transfer Eng.* 23, 3-12.

Zou, Y., Hrnjak, P.S., 2013a. Experiment and visualization on R134a upward flow in the vertical header of microchannel heat exchanger and its effect on distribution. *Int. J. Heat and Mass Trans.* 62, 124-134.

Zou, Y., Hrnjak, P.S., 2013b. Refrigerant distribution in the vertical header of the microchannel heat exchanger - measurement and visualization of R410A flow. *Int. J. Refrigeration.* 36, 2196-2208.

Zou, Y., Hrnjak, P.S., 2014. Effect of oil on R134a distribution in the microchannel heat exchanger with vertical header. Int. J. Refrigeration. *Int. J. Refrigeration.* 40, 201-210.

Zou, Y., Tuo, H., Hrnjak, P.S., 2014. Modeling refrigerant maldistribution in microchannel heat exchangers with vertical headers based on experimentally developed distribution results. *Appl. Thermal Eng.* 64, 172-181.

ACKNOWLEDGEMENT

The authors are grateful for the sponsor and support from the member companies of Air Conditioning and Refrigeration Center at the University of Illinois at Urbana-Champaign.